The Influence of Tidal Currents on the REMUS Autonomous Underwater Vehicle

D. E. Sgarioto
Defence Technology Agency
Devonport Naval Base
Auckland, New Zealand

***Abstract*-This paper outlines the results of an investigation into the influence that tidal currents have on the dynamics, performance and side-scan sonar coverage for the REMUS 100 Autonomous Underwater Vehicle (AUV). The effect that tidal currents have on the vehicle is explored through a number of realistic simulated mine countermeasure operations that cover a wide range of operating scenarios for the vehicle. The representativeness of this modeling capability is established by comparing simulation results with those obtained from field trials. Recommendations for vehicle operation are identified and directions for future work are also provided.**

I. Introduction

This work explores the effect that tidal currents have on the dynamics, performance and side-scan sonar coverage of the REMUS AUV through-

1) The implementation of a time-varying tidal stream current model within a vehicle simulation environment.

2) The integration of Electronic Navigation Chart (ENC)-sourced bathymetry data within the simulation facility.

3) The formulation of a model of the vehicle's side-scan sonar to determine sonar coverage by estimating the area of seabed insonified by the vehicle.

A representative simulation environment for the REMUS AUV has been previously developed. Key components of this simulation capability include a non-linear mathematical model of the vehicle, the implementation of an autonomous vehicle control system and a visualization suite to support and enhance vehicle simulations [1]. The modeling package also contains an optimization-based trim facility, together with a numerical linearization routine for arbitrary flight conditions [2].

It is well known that modeling and simulation can assist with the development of standard operating procedures and appropriate concepts of operations that underlie the proficient tactical use of AUV systems. For example, consider the use of AUVs for route surveying. Often during these missions there are tidal currents whose magnitude and direction are subject to both temporal and spatial variations. The potential impact that currents like these could have on the performance and sonar coverage of the AUV is not well understood. An operator would welcome any useful information regarding the most effective way to task their vehicles given the environmental conditions. It would also be valuable to know beforehand if gaps in sonar coverage can be expected, so that issues such as these can be managed during mission planning.

Figure 1. REMUS 100 vehicle and system components [3].

The REMUS 100 AUV, depicted in Fig. 1, is a slender propeller-driven platform that is deployable by two people from a small boat. The vehicle is operated via commands that are programmed into the computer onboard the vehicle prior to launch. These commands instruct the vehicle to autonomously attain the desired mission objectives. The vehicle maintains the required speed, depth and course using its on-board sensor suite, control algorithms and navigation system, commensurate with the mission plan. The total REMUS 100 system consists of the AUV, supportive mission hardware and software for mission programming and post-mission analysis, all of which are collectively displayed in Fig. 1. The interested reader is referred to [3] for a more thorough treatise of the vehicle's physical characteristics, sensor suite, support equipment, mode of operation, and operational limits.

II. REMUS AUV Modeling

This section introduces the non-linear dynamic model of the REMUS AUV. A derivation of the many elements that comprise the equations of motion for the vehicle will not be presented; only the final result is provided. Alternatively, the reader is directed to [4] and those interested in AUV dynamics and modeling are encouraged to consult [5].

A. *Non-linear Dynamic Vehicle Model*

A submerged underwater vehicle possesses six degrees-of-freedom, three corresponding to translational motion and the remaining three relating to rotational motion. In accordance with standard convention [5], the inertial position η_1, the translational velocity ν_1, the Euler angles η_2 and the angular rates ν_2 for the vehicle are:

978-1-4244-5222-4/10/$26.00 ©2010 CROWN

$$\boldsymbol{\eta}_1=\begin{Bmatrix}\mathrm{X}\\\mathrm{Y}\\\mathrm{Z}\end{Bmatrix},\ \boldsymbol{\nu}_1=\begin{Bmatrix}u\\v\\w\end{Bmatrix},\ \boldsymbol{\eta}_2=\begin{Bmatrix}\phi\\\theta\\\psi\end{Bmatrix},\ \boldsymbol{\nu}_2=\begin{Bmatrix}p\\q\\r\end{Bmatrix} \tag{1}$$

where u is the surge, v is the sway, and w is the heave speed; ϕ is the roll, θ is the pitch, and ψ is the yaw angle; p is the roll rate, q is the pitch rate and r is the yaw rate for the vehicle respectively. The surge equation for translational motion of the vehicle is:

$$\begin{aligned}&m\left[\dot{u}-vr+wq+z_{\mathrm{G}}\left(pr+\dot{q}\right)\right]=\sum X=X_{vr}vr+X_{\dot{u}}\dot{u}+X_{rr}r^2\\&+X_{u|u|}u\left|u\right|+X_{wq}wq+X_{qq}q^2+\left(1-\tau_p\right)T_{n|n|}n\left|n\right|-\left(W-B\right)\sin\theta\end{aligned} \tag{2}$$

The equation for sway motion is:

$$\begin{aligned}&m\left[\dot{v}-wp+ur+z_{\mathrm{G}}\left(qr-\dot{p}\right)\right]=\sum Y\\&=\left(W-B\right)\cos\theta\sin\phi+Y_{uv}uv+Y_{v|v|}v\left|v\right|+Y_{r|r|}r\left|r\right|\\&+Y_{\dot{v}}\dot{v}+Y_{\dot{r}}\dot{r}+Y_{ur}ur+Y_{wp}wp+Y_{pq}pq+Y_{uu\delta_r}u^2\delta_r\end{aligned} \tag{3}$$

The heave motion equation for the AUV is:

$$\begin{aligned}&m\left[\dot{w}-uq+vp-z_{\mathrm{G}}\left(p^2+q^2\right)\right]=\sum Z\\&=\left(W-B\right)\cos\theta\cos\phi+Z_{\dot{w}}\dot{w}+Z_{\dot{q}}\dot{q}+Z_{uq}uq+Z_{vp}vp\\&+Z_{rp}rp+Z_{w|w|}w\left|w\right|+Z_{q|q|}q\left|q\right|+Z_{uw}uw+Z_{uu\delta_s}u^2\delta_s\end{aligned} \tag{4}$$

The equation for roll motion is:

$$\begin{aligned}&I_{xx}\dot{p}+\left(I_{zz}-I_{yy}\right)qr-mz_{\mathrm{G}}\left(\dot{v}-wp+ur\right)=\sum K\\&=-z_{\mathrm{G}}W\cos\theta\sin\phi+K_{\dot{p}}\dot{p}+K_{p|p|}p\left|p\right|+Q_{n|n|}n\left|n\right|\end{aligned} \tag{5}$$

The equation for pitch motion is:

$$\begin{aligned}&I_{yy}\dot{q}+\left(I_{xx}-I_{zz}\right)rp+mz_{\mathrm{G}}\left(\dot{u}-vr+wq\right)=\sum M\\&=-z_{\mathrm{G}}W\sin\theta+M_{\dot{w}}\dot{w}+M_{\dot{q}}\dot{q}+M_{uw}uw+M_{vp}vp\\&+M_{rp}rp+M_{uq}uq+M_{w|w|}w\left|w\right|+M_{q|q|}q\left|q\right|+M_{uu\delta_s}u^2\delta_s\end{aligned} \tag{6}$$

The yaw equation of motion for the vehicle is:

$$\begin{aligned}&I_{zz}\dot{r}+\left(I_{yy}-I_{xx}\right)pq=\sum N=N_{uv}uv+N_{wp}wp+N_{pq}pq\\&+N_{ur}ur+N_{v|v|}v\left|v\right|+N_{r|r|}r\left|r\right|+N_{uu\delta_r}u^2\delta_r+N_{\dot{v}}\dot{v}+N_{\dot{r}}\dot{r}\end{aligned} \tag{7}$$

The ground speed equations for the vehicle are given by:

$$\begin{aligned}\dot{\mathrm{X}}&=\left(\mathrm{c}\psi\,\mathrm{c}\theta\right)u+\left(\mathrm{c}\psi\,\mathrm{s}\theta\,\mathrm{s}\phi-\mathrm{s}\psi\,\mathrm{c}\phi\right)v+\left(\mathrm{s}\psi\,\mathrm{s}\phi+\mathrm{c}\psi\,\mathrm{s}\theta\,\mathrm{c}\phi\right)w\\\dot{\mathrm{Y}}&=\left(\mathrm{s}\psi\,\mathrm{c}\theta\right)u+\left(\mathrm{c}\psi\,\mathrm{c}\phi+\mathrm{s}\psi\,\mathrm{s}\theta\,\mathrm{s}\phi\right)v+\left(\mathrm{s}\psi\,\mathrm{s}\theta\,\mathrm{c}\phi-\mathrm{c}\psi\,\mathrm{s}\phi\right)w\\\dot{\mathrm{Z}}&=\left(-\mathrm{s}\theta\right)u+\left(\mathrm{c}\theta\,\mathrm{s}\phi\right)v+\left(\mathrm{c}\theta\,\mathrm{c}\phi\right)w\end{aligned} \tag{8}$$

where $\mathrm{c}(.)$ and $\mathrm{s}(.)$ are abbreviations for sine and cosine respectively. The Euler rate equations for the AUV are:

$$\begin{aligned}\dot{\phi}&=p+\left(\sin\phi\tan\theta\right)q+\left(\cos\phi\tan\theta\right)r\\\dot{\theta}&=\left(\cos\phi\right)q+\left(-\sin\phi\right)r\\\dot{\psi}&=\left(\sin\phi/\cos\theta\right)q+\left(\cos\phi/\cos\theta\right)r\end{aligned} \tag{9}$$

The AUV's thruster equations of motion are given by [6]:

$$\begin{aligned}&J_m\dot{n}+K_n n=Q-Q_{n|n|}n\left|n\right|\\&m_f\dot{u}_p=T_{n|n|}n\left|n\right|-d_{f_0}u_p-d_f\left|u_p\right|\left[u_p-\left(1-w_p\right)u\right]\end{aligned} \tag{10}$$

where n is the propeller shaft speed, u_p is the inflow velocity through the propeller, and d_{f_0} and d_f are the linear and quadratic damping coefficients (see [6]). The parameters governing the equations of motion can be found in [4]. Equation (2) through to (10) represent the complete set of equations that govern the dynamics of the AUV, recast in state space form as:

$$\dot{\mathbf{x}}(t)=\boldsymbol{f}\left[\mathbf{x}(t),\mathbf{u}(t),t\right] \tag{11}$$

where $\mathbf{x}(t)$ and $\mathbf{u}(t)$ are the corresponding state and control vectors for the vehicle. The actuators chosen to control the dynamics of the vehicle are the propeller torque Q and the displacement of the elevator δ_s and rudder δ_r.

B. Accounting for Time-Varying Tidal Currents

The content of this section has been adapted from material presented by Healey [7]. By invoking the irrotational flow assumption, time-varying tidal currents are accounted for by assuming that all local water particles have a relative translational velocity with respect to the global reference frame (ignoring the downward water column component):

$$\mathbf{U}_c=\left\{\mathrm{U}_c\quad \mathrm{V}_c\quad 0\right\}^T \tag{12}$$

Furthermore, the velocity of the vehicle in the body-fixed frame is now defined to be the vehicle velocity relative to the water, expressed in body-fixed coordinates as:

$$\boldsymbol{\nu}_{r_1}=\left\{u_r\quad v_r\quad w_r\right\}^T=\left\{\left(u-u_c\right)\quad\left(v-v_c\right)\quad w\right\}^T \tag{13}$$

Now the absolute velocity terms that appear in the equations of motion for the vehicle are replaced with these relative velocity components. Since the tidal currents are prescribed in the inertial frame, they are required to be reformulated in the vehicle's body-fixed frame. The vehicle's translational velocity in the body-fixed frame is related to that in the inertial frame by the orthogonal coordinate transformation matrix $\boldsymbol{J}_1$:

$$\boldsymbol{J}_1(\boldsymbol{\eta}_2)=\begin{bmatrix} c\psi c\theta & -s\psi c\phi + c\psi s\theta s\phi & s\psi s\phi + c\psi s\theta c\phi \\ s\psi c\theta & c\psi c\phi + s\psi s\theta s\phi & -c\psi s\phi + s\psi s\theta c\phi \\ -s\theta & c\theta s\phi & c\theta c\phi \end{bmatrix} \quad (14)$$

Therefore, the tidal currents expressed in the vehicle's body-fixed frame are:

$$\mathbf{u}_c = \{u_c \quad v_c \quad 0\}^T = \boldsymbol{J}_1 \mathbf{U}_c \quad (15)$$

The excitation loads $\mathbf{f}_c$ that the time-varying currents produce for the vehicle manifest as Froude-Krylov forces (pressure induced) and rigid body inertia forces given by:

$$\mathbf{f}_c = \{X_c \quad Y_c \quad Z_c \quad K_c \quad M_c \quad N_c\}^T = \mathbf{M}_{fkrb}[\dot{\boldsymbol{J}}\mathbf{U}_c + \boldsymbol{J}_1\dot{\mathbf{U}}_c] \quad (16)$$

where $\dot{\mathbf{U}}_c$ is the time rate of change of the tidal currents and $\dot{\boldsymbol{J}}$ the time rate of change of the transformation matrix, which can be expressed as [7]:

$$\dot{\boldsymbol{J}} = \begin{bmatrix} 0 & -r & q \\ r & 0 & -p \\ -q & p & 0 \end{bmatrix}^T \boldsymbol{J}_1 \quad (17)$$

The matrix $\mathbf{M}_{fkrb}$ is composed of the Froude-Krylov mass $\mathbf{M}_{fk}$ and rigid body inertia $\mathbf{M}_{rb}$ matrices for the vehicle, formulated using:

$$\mathbf{M}_{fkrb} = \mathbf{M}_{fk} - \mathbf{M}_{rb} = \begin{bmatrix} \frac{(B-W)}{g} & 0 & 0 & 0 & 0 & 0 \\ 0 & \frac{(B-W)}{g} & 0 & 0 & 0 & 0 \\ 0 & 0 & \frac{(B-W)}{g} & 0 & 0 & 0 \\ 0 & \frac{Wz_g}{g} & 0 & 0 & 0 & 0 \\ -\frac{Wz_g}{g} & 0 & 0 & 0 & 0 & 0 \\ 0 & 0 & 0 & 0 & 0 & 0 \end{bmatrix} \quad (18)$$

where B and W are the buoyancy and gravitational forces acting on the vehicle and z_g is the vertical separation between the centers of gravity and buoyancy. Since it is assumed that the rotational motion of the current is zero, coriolis and centrifugal forces are not included in the formulation of the Froude-Krylov forces and moments. Inclusion of the appropriate components of (16) into the right hand side of the relevant equations of motion for the vehicle then enables the motion of the time-varying tidal currents to be accounted for within the vehicle simulation model.

Finally, the vehicle ground speed equations given by (8) are modified to include the variable magnitude current velocity components as follows:

$$\begin{aligned} \dot{X} &= (c\psi c\theta)u + (c\psi s\theta s\phi - s\psi c\phi)v + (s\psi s\phi + c\psi s\theta c\phi)w + U_c \\ \dot{Y} &= (s\psi c\theta)u + (c\psi c\phi + s\psi s\theta s\phi)v + (s\psi s\theta c\phi - c\psi s\phi)w + V_c \\ \dot{Z} &= (-s\theta)u + (c\theta s\phi)v + (c\theta c\phi)w \end{aligned} \quad (19)$$

C. *REMUS AUV Control*

The REMUS AUV control system design (see [1] for details) is based on the decoupled controller design paradigm, whereby a set of separate designs for speed, steering and diving control are obtained, in-line with conventional AUV control design philosophy [8].

The speed control autopilot for the REMUS AUV is a conventional Proportional-Integral (PI) controller that uses an error signal based on the motor/propeller rotational speed, with the control input itself being the commanded mechanical torque of the thruster motor. A Proportional-Integral-Derivative (PID)-type controller forms the basis of the vehicle's diving autopilot. This controller ensures that the vehicle maintains a particular depth, or if required, commands the vehicle to track the sea floor at a constant altitude.

The steering autopilot for the vehicle is a complex hybrid controller. Its simplest form is a Proportional-Derivative (PD) controller used to command the vehicle to loiter about a desired location. The remaining two variants of the controller are dependent on the magnitude of the vehicle's heading error. For large heading errors, the steering autopilot constitutes a PD-type feedback controller, in conjunction with Line Of Sight (LOS) guidance. This is supplemented with a follow-the-rabbit technique that is similar to the transducer-based dead-reckoning approach the actual vehicle implements in the field [9]. Small heading errors are corrected by a controller based on the Cross Track Error (CTE) of the vehicle. These steering autopilots, together with the guidance and navigation system for the REMUS AUV, are closely based on similar systems developed by Marco and Healey for the Naval Postgraduate School (NPS) ARIES AUV [10].

Wherever the vehicle's control system utilizes integral action, to prevent windup, the integrators are reset to zero and integral control action is disabled if the relevant control input becomes saturated. In order to ensure that REMUS AUV simulations remain representative across the total performance envelope of the vehicle, the control gains for the vehicle's autopilots are scheduled with respect to the vehicle's velocity.

III. ENVIRONMENTAL MODELING

A. *Tidal Currents*

The tidal current model used in this study is based on the Princeton Ocean Model (POM) [11]. POM has been applied to a portion of the North East coast of the North Island of New Zealand to predict the characteristics of tidal currents at locations of up to 150 nautical miles off the coast. The spatial resolution of the model is 2 hundredths of a degree latitude and longitude (approximately 2 kilometers), with data quoted in 15 minute intervals 12 hours either side of high tide. Temporal data is relative to high water times in the city of Auckland and tidal currents consistent with both spring and neap conditions are available. Tidal stream velocities are depth averaged and directions are quoted as nautical degrees from True North.

Prior to initiating a simulation, both the local time for mission commencement and the time for high-water (HW) in Auckland need to be determined. Similarly, the data point within the model that is closest to the geographical centre of the mission operational area (OPAREA) is then located. Using this data point and the "mission start-Auckland HW" temporal offset, nearest neighbor interpolation is employed to determine magnitude and direction of the current as the simulation progresses. The time-rate of change of the tidal current velocity is critical to the inclusion of time-varying currents within the REMUS model. Since the spatial resolution of the model is relatively coarse, calculating the partial derivatives with respect to vehicle position necessary for $\dot{\mathbf{U}}_c$ is not warranted. Instead, the current velocity derivative with respect to time is estimated off-line using a simple finite differencing routine.

B. Sea Floor Terrain

In general, the profile of real sea floor terrain is complex, and in order to appropriately account for generic terrain profiles during a simulation, a discrete point mapping approximation has been developed. This routine consists of three steps, only one of which is executed on-line during a simulation.

Firstly, a source of bathymetry data relevant to a particular simulation needs to be acquired. Whilst many such sources are possible, in this work, the depth soundings from an appropriate ENC are utilized. ENCs, produced according to the International Hydrographic Organization (IHO) S-57 standard, are vector-based digital maps specifically designed for maritime navigation. Unfortunately, the manner in which depth sounding data is handled by the S-57 standard is not well suited for use as part of a sea floor terrain approximation scheme, since one sounding feature can have many sounding points associated with it.

As a result, the raw sounding layers from a candidate ENC need to be extracted and outputted as an ASCII text data set or similar data format comprised solely of latitude, longitude and depth readings. The easiest way to do this is to use a Geospatial Information System (GIS) to view the ENC and then export the sounding layers as appropriate.

The second step constitutes a matrix approximation measure. The pre-processed sounding data is obtained as a set comprising of latitude, longitude and water column depth. The vehicle's latitude and longitude are first converted to global Cartesian coordinates and then processed using John D'Errico's "GRIDFIT" algorithm [12], which outputs a sea floor terrain matrix in the required form necessary for use within the forthcoming matrix interpolation routine. The GRIDFIT matrix approximation algorithm fits a smooth surface to the scattered original bathymetry data, allowing for both noise and replicate data.

Unlike the previous two steps, which are carried out off-line prior to the commencement of a simulation, the final process involved in approximating the topography of real sea floor surfaces is on-line matrix interpolation. Here, Long and Long's Singular Value Decomposition (SVD) technique [13] is utilized to extend planar function interpolation into three dimensions. This enables the elevation of the seabed to be determined for any given position of the vehicle within the prescribed OPAREA. The method is inherently simple and easy to implement, and relatively quick provided the matrix of terrain data has a low rank or a low rank approximation may be used without compromising the fidelity of the technique.

C. Side-scan Sonar

In order to attain an appreciation for how tidal currents have the potential to affect the side-scan sonar coverage provided by the vehicle, a model of the vehicle's side-scan sonar has been developed. This model is a highly idealized, geometrical optics model of the vehicle's sonar, which attempts to quantify "coverage" by determining the projection the vehicle's sonar beams make onto the sea floor. It is assumed that the sea floor is flat and that underwater acoustic phenomena such as noise, diffraction, transmission loss, scattering, spreading and absorption can be ignored. The resulting coverage levels predicted by the model are likely to be optimistic. However, the near nadir region and the influence of the vehicle's attitude on the orientation of the sonar beams are accounted for in the model. Fig. 2 presents a graphical depiction of the REMUS AUV side-scan sonar model. The area of seabed insonified by the vehicle is represented as a mosaic image that is constructed in much the same manner as waterfall displays are created by the side-scan sonar system on-board the vehicle *i.e.* a composition of numerous "swaths" taken at regular intervals during a simulation.

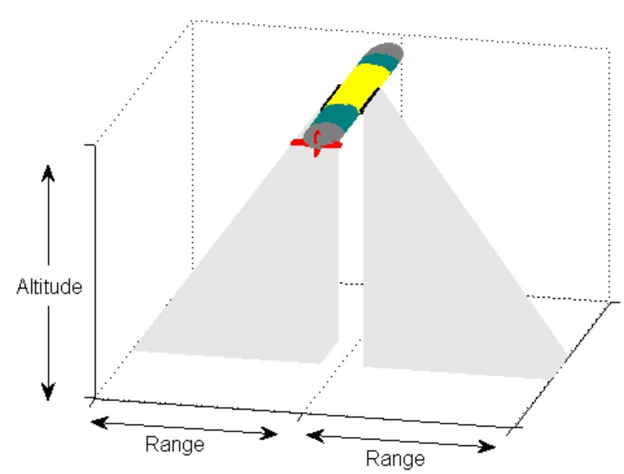

Figure 2. Depiction of REMUS AUV side-scan sonar model.

IV. Results

This section outlines a series of demonstrative case study scenarios. Initially, the representativeness of the virtual REMUS modeling environment is established by comparing simulation results with those garnered in the field. Through a sequence of realistic REMUS MCM missions, the effect that tidal currents have on both the performance of the vehicle itself, and the expected level of sonar coverage it can provide, is then offered.

A. *Validation*

The REMUS AUV field data used for the validation exercise was obtained by members of the Defence Science and Technology Organisation's (DSTO) Maritime Operations Division during DUGONG 07 Trials in the Spencer Gulf region of South Australia [14]. Drift rates when the vehicle was on surface obtaining GPS fixes indicated that tidal flows of approximately 1 knot in a westerly direction (270° from true North) were present. The mission consisted of a series of Re-acquire and Identify (RAI) missions, but only the first RAI maneuver will be considered, since the results observed were representative of the remaining RAI missions.

The trajectory of the vehicle as predicted by the simulation model and that recorded by the actual vehicle is presented in Fig. 3. The differences between the real trajectory and that predicted by the model are few, indicating that the trajectories predicted via simulation are feasible and consistent with that expected of a real vehicle. The real vehicle suffers from a greater degree of overshoot after turns compared to the model. Immediately after the start of the mission, the real vehicle can be seen to take much longer to turn against the current than the simulated model. This is due to the fact that the actual vehicle commences the mission at rest on the surface, whereas the vehicle model is assumed to be in steady-level flight prior to the mission. The reason why the real vehicle does not initially head towards the second waypoint is unknown, so too is the large heading alteration the real vehicle executes when transitioning between the second and third waypoints.

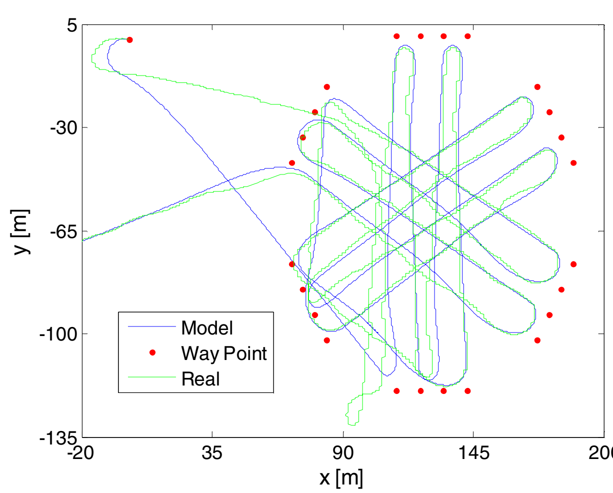

Figure 3. Comparison between simulated and real vehicle trajectories.

B. *Case Study Examples*

The scope of the subsequent analysis is limited to exploring the effect that tidal currents have on both the dynamics and performance of the vehicle, as well as the level of sonar coverage the REMUS can provide. The simulations will focus on typical mine-hunting missions the vehicle is requested to execute during mine countermeasures operations, so-called Search-Classify-Map (SCM) and Re-Acquire and Identify missions, using both in-going and out-going tidal stream scenarios.

The OPAREA chosen for the simulation case studies is a 1000 m by 400 m region within the western channel of Tauranga Harbor, a frequent training and trial staging area for the Royal New Zealand Navy (RNZN) REMUS operators. The OPAREA has a maximum depth of 7 m at low water and a tidal range of approximately 2 m. The OPAREA also experiences a flood/ebb tidal stream of 2 knots (spring tide conditions), equal to the recommended maximum operating water current for the REMUS 100 AUV. The ebb and flood tidal streams are qualitatively similar in nature and differ only with respect to the direction in which they prevail relative to the vehicle. Fig. 4 details the topography of the seafloor within the chosen OPAREA, together with the direction of the prevailing tidal streams.

The initial condition chosen to commence the simulations for the case studies was the equilibrium condition of the vehicle travelling steady and level at a speed of 4 knots just below the surface.

1) *Search Classify Map Missions*: the first group of case study simulations involve two variants of a SCM mission, each of which will be separately considered. Each simulation (a total of four) spans approximately 50 minutes either side of the largest peaks that occur for both an in-coming and out-going tide. The current is slightly stronger in magnitude during the ebb tide.

The vehicle search pattern proposed for the SCM Variant 1 mission is outlined in Fig. 5.

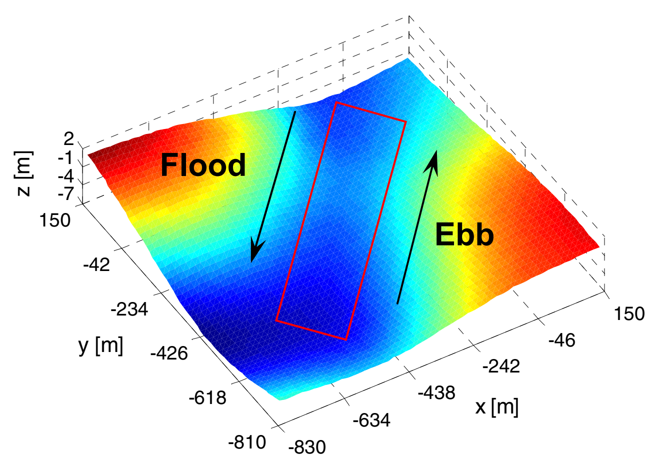

Figure 4. Vehicle OPAREA utilized for simulated case study examples.

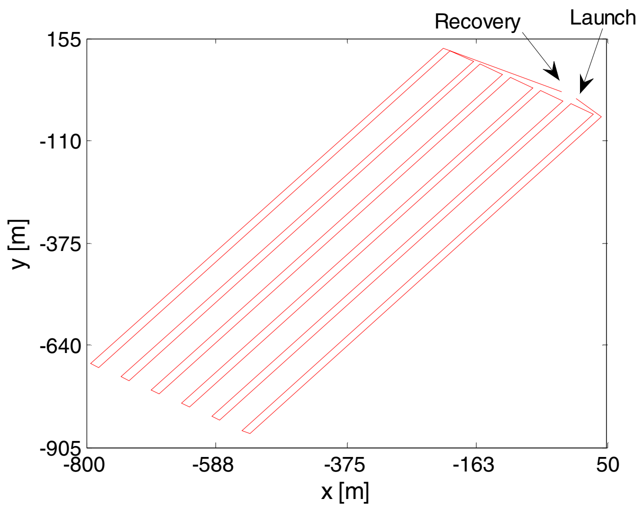

Figure 5. Proposed vehicle search pattern for SCM variant 1 mission.

During this mission, the vehicle travels mostly parallel to the nominal direction of the tidal stream. The mission consists of 12 legs that are 1000 m long, with the track spacing alternating between 15 and 40 m. This track spacing produces sufficient overlap to ensure that the search area is completely covered by the vehicle's side-scan sonar. The search and transit speeds of the vehicle are 3 and 4 knots respectively. The altitude for the vehicle is prescribed at 3 m and a sonar range of 30 m is employed. The vehicle is initially positioned at the first waypoint (Launch) and has an initial heading in the direction of the tidal stream. Once the vehicle has completed the nominated search, it returns to a location in the vicinity of its launch point and ascends to the surface (Recovery).

The effect that both flood and ebb tidal streams have on the trajectory of the vehicle during the SCM Variant 1 mission is shown in Fig. 6. When the vehicle travels along the 1000 m long rows, the tidal streams produce CTEs in the order of 1 m.

Perturbations of up to 13 m were observed when the vehicle transitioned between neighboring waypoints. The large reduction in speed the vehicle experiences during turns is the reason these large deviations are forced upon the vehicle. However, the vehicle was able to complete the proposed mission successfully in spite of the adverse impact that the currents impose on the vehicle. As expected, the stronger ebb tide induced slightly larger CTEs for the vehicle, yet Fig. 6 indicates that the flood stream had more of an effect on the vehicle whilst turning.

The area of sonar coverage undergoes a clear shift to the North-North East when the tide is ebbing and a comparable South-South West shift occurs as a result of the in-coming tide. Encouragingly, irrespective of the tide scenario, there were no observed gaps in the sonar coverage provided by the vehicle upon completion of the SCM mission. However, closer inspection of the sonar mosaics indicates that both tidal streams did reduce the number of times many areas of the seabed were insonified. The areas where this reduced insonification occurred were mainly located in the vicinity of the midline between adjacent legs. Fig. 7 details an example of one of theses areas of reduced seabed insonification (region bounded by green lines). An area of seabed approximately 3 m wide and almost spanning the entire length of a row was imaged by the vehicle's sonar once instead of the two times that was commensurate with the mission plan. Consistent with the finding that the ebb tide induced slightly larger cross track errors for the vehicle, the areas of reduced seabed insonification were marginally larger during an out-going tide than those observed during the flood tide.

The search pattern that constitutes the SCM Variant 2 mission is displayed in Fig. 8. During this mission, the vehicle mostly travels perpendicular to the nominal direction of the tidal stream. The mission consists of 36 legs that are 315 m long, with the track spacing again alternating between 15 and 40 m to ensure sufficient overlap.

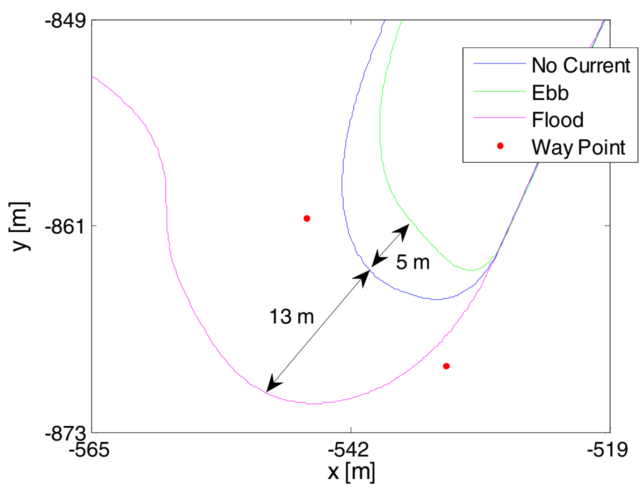

Figure 6. Influence of tidal currents on vehicle during SCM variant 1 mission.

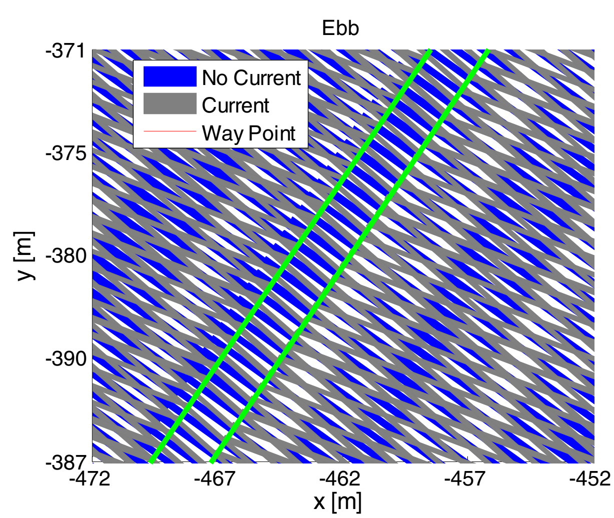

Figure 7. Example of reduced seabed insonification during SCM variant 1 mission for ebb tide conditions.

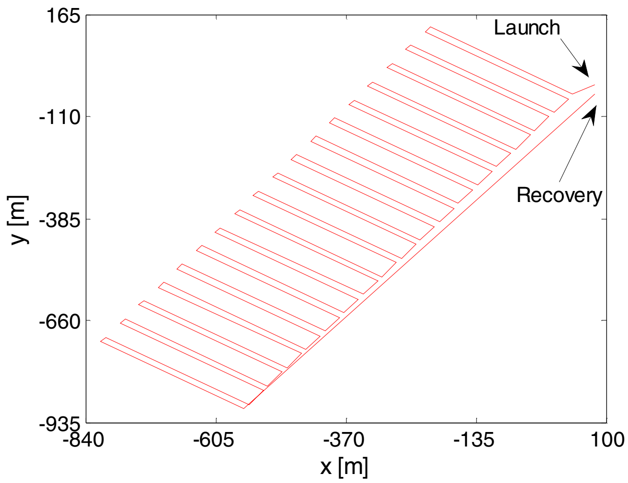

Figure 8. Proposed vehicle search pattern for SCM variant 2 mission.

The search and transit speeds of the vehicle are once again 3 and 4 knots respectively and the same altitude (3 m) and sonar range (30 m) employed during the previous mission are utilized for this SCM mission.

The impact that both tidal streams have on the trajectory of the vehicle during the SCM Variant 2 mission is revealed in Fig. 9. Since the vehicle was mostly travelling perpendicular to the current, as expected, the CTEs in this mission (approximately 7 m) were much larger than those the vehicle experienced in the previous SCM mission (approximately 1 m). Like the previous SCM variant, the flood stream also had more of an effect on the maneuvering vehicle during this mission: perturbations of up to 16 m were experienced by the vehicle during turns. However, irrespective of the direction of the tide, the vehicle was still able to successfully complete the proposed SCM Variant 2 mission.

The influence that the tidal streams had on the vehicle sonar coverage for this mission is depicted in Fig. 10.

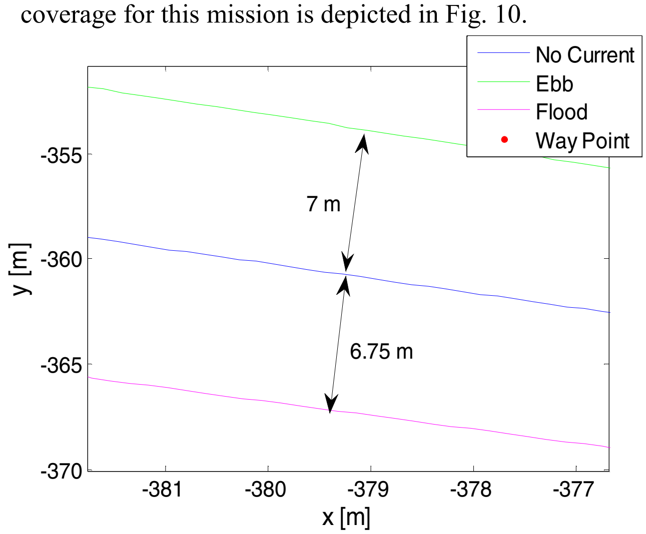

Figure 9. Influence of tidal currents on vehicle cross track error during SCM variant 2 mission.

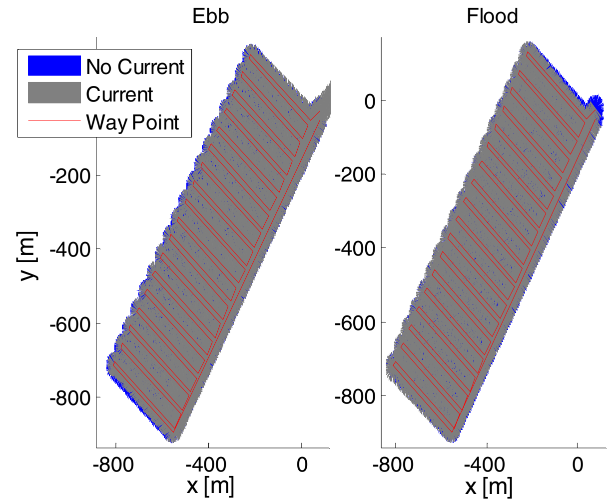

Figure 10. Influence of tidal currents on vehicle sonar coverage for SCM variant 2 mission- (a) ebb tide (b) flood tide.

Like the previous SCM mission, a clear shift in the sonar coverage to the North-North East occurs when the tide is ebbing, with an analogous South-South West shift arising as a consequence of the flood tide. However, there were no gaps observed in the vehicle's sonar coverage regardless of the direction of the tide. Yet like the previous SCM mission, the tidal streams were found to reduce the number of times many areas of the seabed were insonified. In general, these areas were significantly wider and shorter in length than those typical of the previous SCM mission, but in terms of total area, they were somewhat larger (approximately 20 %). Consequentially, the results presented in this sub-section support the widely held view that when significant tidal flows are encountered, search patterns similar to Fig. 5 (vehicle traveling mostly parallel to the current) are preferable to those characteristic of Fig. 8 (vehicle travelling nominally perpendicular to the tidal stream).

2) *Re-acquire and Identify Missions*: The final set of case study simulations consist of Reacquire and Identify missions performed on three targets. The vehicle search pattern proposed for the RAI missions is outlined in Fig. 11. During this mission, the vehicle performs a detailed search over three target locations. For each target, the vehicle obtains 3 "views" using 4 rows that are 120 m long and spaced 10 m apart. The search and transit speeds of the vehicle are 4 and 4.5 knots respectively, whilst the altitude and sonar range for the vehicle are prescribed at 3 m and 10 m respectively. The vehicle is initially positioned at the first waypoint and has an initial heading in the direction of the tidal stream. Once the vehicle has completed the RAI maneuvers, it transits to a position near the launch location and surfaces. The tidal current dynamics are the same as those utilized for the SCM simulations, except that these simulations span only 25 minutes either side of the peaks that occur for both ebb and flood tides.

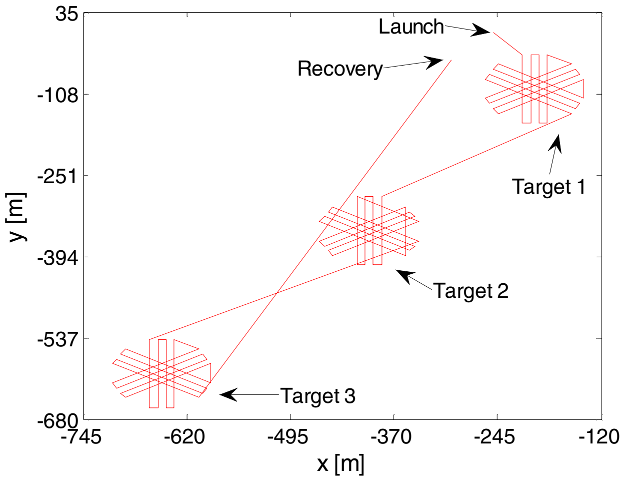

Figure 11. Proposed vehicle search pattern for RAI mission.

Using as an example the portion of the mission corresponding to the vehicle maneuvering over Target 3, the effect that both tidal streams have on the trajectory of the vehicle during the RAI mission is detailed in Fig. 12. It can be seen for Fig. 12 that the North West-South East legs of the mission are particularly impacted by the action of the tidal streams. Like the previous SCM missions, generally the CTE induced by the tidal streams is slightly larger during the out-going tide, though large CTEs are experienced by the vehicle during the in-coming tide, especially throughout the North West-South East legs of the mission. Once again, it was observed that the flood stream had more of an effect on the maneuvering vehicle, where perturbations of up to 14 m are experienced by the vehicle during turns. However, irrespective of the direction of the tide, the vehicle was successfully able to complete the mission as planned. A clear shift in the vehicle's track to the North-North East occurs during the ebb tide, with a comparable South-South West shift taking place due to the in-coming tide.

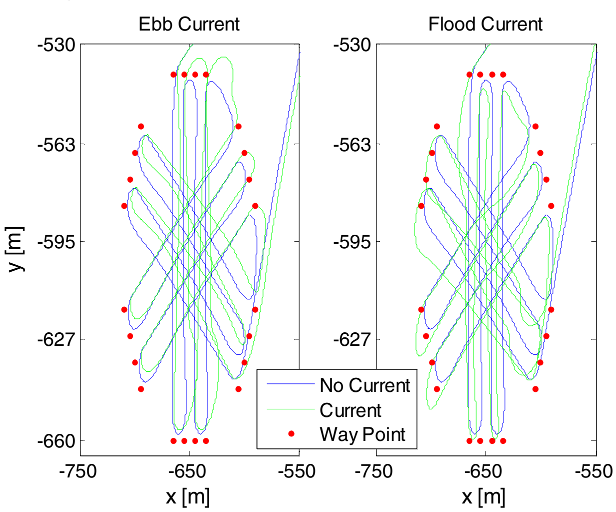

Figure 12. Influence of tidal currents on vehicle trajectory during RAI mission over Target 3- (a) ebb tide (b) flood tide.

During RAI maneuvers, it is not unusual to operate the REMUS with a vehicle search speed of 3 knots. However, if this parameter is utilized for the proposed RAI mission, the 2 knot tidal streams prevent the vehicle from successfully completing the mission. In order for the vehicle to accommodate the potentially large impact that currents can have on its performance, it is advisable that both the vehicle's search and transit speeds be sufficiently larger than (in the order of 2 knots) the magnitude of any prevailing currents.

Fig. 13 depicts the influence that the tidal streams have on the sonar coverage achieved by the vehicle throughout the RAI missions. Unlike the previous SCM missions, Fig. 13 indicates that both the ebb and flood tidal streams cause numerous gaps in the sonar coverage (regions enclosed by yellow circles in Fig. 13). These gaps range from 0.5 to up to 30 m^2, an example of which is provided by Fig. 14.

There was no clearly identifiable relationship between the size of the gaps in the sonar coverage and the nominal direction of the tide, though the gaps are clustered towards the Northern end of each RAI maneuver and occur as close as 45 m from the target location. Fortunately, this places all of these gaps well outside the range of GPS error, however the proximity of these gaps to target locations is also strongly influenced by human error and other uncertainties associated with transponder deployment. Consequently, there may be scenarios in which these sonar gaps are effectively placed much closer to the target to make them more of a concern to REMUS mission planners and operators. Similarly, the tidal streams not only produce gaps in sonar coverage, but as experienced during the previous SCM missions, they also reduce the number of times many areas of the seabed are insonified. Much like the gaps themselves, there was no clearly identifiable relationship between the size of these areas of reduced insonification and the nominal direction of the tide.

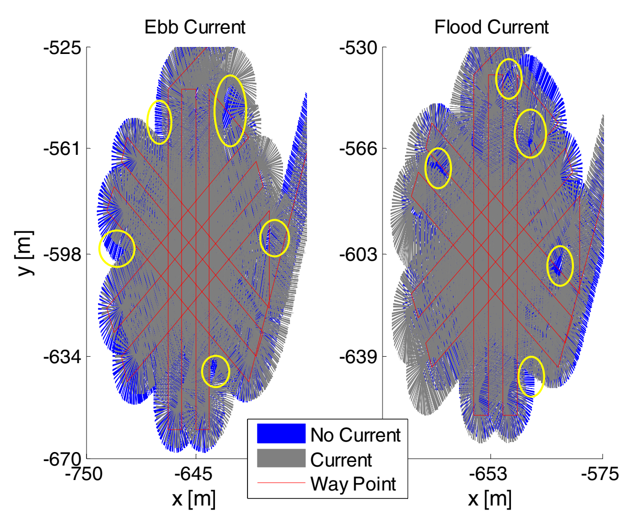

Figure 13. Influence of tidal currents on vehicle trajectory during RAI mission over Target 3- (a) ebb tide (b) flood tide.

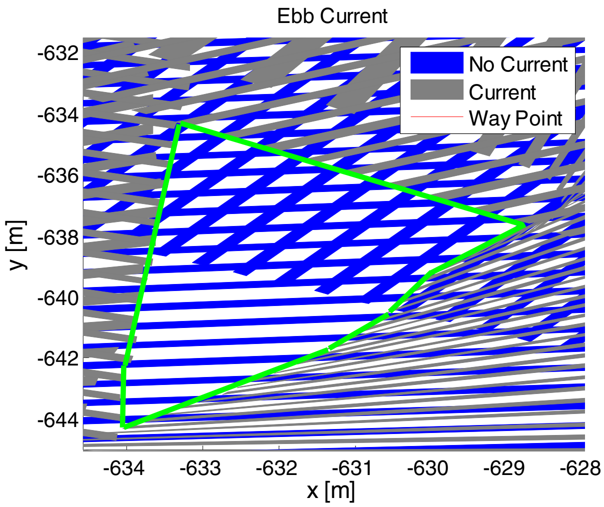

Figure 14. Example of gap in sonar coverage during RAI mission for ebb tide conditions.

In light of these considerations, increasing the number of rows and views of a target may be necessary to achieve the required level of sonar coverage when the vehicle is to be deployed in areas where sizable tidal streams are prevalent.

V. Conclusions

The results obtained indicate that the vehicle was successfully able to complete the proposed SCM and RAI missions despite the adverse impacts that the tidal streams imposed on the vehicle. Each tidal stream was found to induce sizable cross track errors for the vehicle during all missions. As expected, when the vehicle was mostly travelling perpendicular to the prevailing tidal stream, the cross track errors were much larger.

Upon completion of all SCM missions, there were no observed gaps in the sonar coverage provided by the vehicle. However, close inspection of the sonar coverage indicated that both tidal streams did reduce the number of times many areas of the seabed were insonified. These areas were larger during SCM missions where the vehicle travelled mostly perpendicular to the current. This suggests that search patterns that compel the vehicle to travel mostly parallel to the current are preferable to those where the direction of travel is generally perpendicular to the tidal stream. Similarly, so that the vehicle can resist the adverse influence of currents, it is prudent to ensure the vehicle's speed is sufficiently larger than the magnitude of any prevailing tidal stream. In contrast to the SCM missions, numerous gaps were observed in the vehicle's sonar coverage during the RAI missions, some as large as 30 m^2 and occurring as close as 45 m from target locations. These gaps may be sufficiently far enough away from target locations to be of much concern to vehicle operators. However, the proximity of these gaps to target locations is also strongly influenced by human error and other operational uncertainties. Furthermore, tidal streams also reduced the number of times many areas of the seabed were insonified during the RAI missions. Therefore, it may be necessary to increase the number of rows and views of a target to achieve the required level of sonar coverage, if the vehicle is deployed in areas where sizable tidal streams are prevalent

VI. Further Work

There is sufficient scope to further develop the tidal current model that is utilized to predict how the vehicle interacts with time-varying tidal streams. Greater coverage of the coast line and an increase to the spatial resolution for inshore areas are obvious candidates for improvement. Validated sources of tidal data and additional validation work covering a wider range of operating conditions also represent opportunities for further research.

Acknowledgment

The author would like to thank Dr. Reinhard Holtkamp for his helpful discussions and useful feedback. The valuable insights, comments and REMUS 100 trial data provided by Michael Bell and Dr. Stuart Anstee from the Maritime Operations Division, DSTO Sydney is also acknowledged.

References

[1] D. E. Sgarioto, "Control system design and development for the REMUS autonomous underwater vehicle," in *Proceedings of the Undersea Defence Technology Pacific Conference (UDT Pacific 2008)*, Sydney, Australia, Nov. 4-6, 2008, pp. 1-20.

[2] D. E. Sgarioto, "Steady state trim and open loop stability analysis for the REMUS autonomous underwater vehicle," in *Proceedings of the 7th International Conference on Control and Automation (ICCA'09)*, Christchurch, New Zealand, Dec. 9-11, 2009, pp. 1597-1602.

[3] Hydroid LLC., "REMUS 100 operations and maintenance manual," Revision 7.2, Oct 2006.

[4] T. Prestero, "Verification of a six-degree-of-freedom simulation model for the REMUS autonomous underwater vehicle," M.S. Thesis, Dept. Mech. Eng., MIT, Cambridge, MA, Sept. 2001.

[5] T. I. Fossen, *Guidance and Control of Ocean Vehicles*. New York: John Wiley & Sons, 1994.

[6] M. Blanke, K. P. Lindergaard, and T. I. Fossen, "Dynamic model of thrust generation for marine propellers," in *IFAC Conference on Manoeuvring and Control of Marine Craft*, Aalbourg, Denmark, 2000, pp. 23-28.

[7] A. J. Healey, "Dynamics and control of mobile robotic vehicles," Monterey: Naval Postgraduate School Lecture Notes, 2001.

[8] A. J. Healey and D. Lienard, "Multivariable sliding-mode control for autonomous diving and steering of unmanned underwater vehicles," *IEEE Journal of Oceanic Engineering,* vol. 18, no. 3, pp. 327-339, Jul. 1993.

[9] L. R Fodrea, "Obstacle avoidance control for the REMUS autonomous underwater vehicle", MSc. Thesis, Naval Postgraduate School, Monterey, CA, Dec. 2002.

[10] D. B. Marco and A. J. Healey, "Command, control and navigation experimental results with the NPS Aries AUV," *IEEE Journal of Oceanic Engineering,* vol. 26, no. 4, pp. 466-477, Oct. 2001.

[11] A. F. Blumberg and G. L. Mellor, "A description of a three-dimensional coastal ocean circulation model," in *Three-Dimensional Coastal Ocean Models*. vol. 1-16, N. S. Heaps, Ed. Washington DC: American Geophysical Union, 1987.

[12] J. R. D'Errico, "Understanding GRIDFIT," self published, 2006.

[13] A. E. Long and C. A. Long, "Surface approximation and interpolation via matrix SVD," *College Mathematics Journal,* vol. 32, pp. 20-25, 2001.

[14] M. Bell, "Trials Report- DUGONG 07 Whyalla, November 2007", Maritime Operations Division, Defence Science and Technology Organisation, Pyrmont, New South Wales, 2007.